Available online at www.sciencedirect.com
SCIENCE DIRECT®
Journal of Molecular Catalysis A: Chemical 221 (2004) 163–168
JOURNAL OF MOLECULAR CATALYSIS A: CHEMICAL
www.elsevier.com/locate/molcata

Characterization and reactivity of SnO_2-doped V_2O_5/γ-Al_2O_3 catalysts in dehydrogenation of isobutane to isobutene

Yinghuan Fu, Hongchao Ma, Zhenlü Wang, Wanchun Zhu, Tonghao Wu, Guo-jia Wang*

Department of Chemistry, Jilin University, Changchun 130023, PR China

Received 3 April 2004; received in revised form 6 July 2004; accepted 6 July 2004
Available online 26 August 2004

Abstract

Alumina-supported vanadium oxide catalysts ($V_2O_5 \sim 10$ wt.%) with and without SnO_2 were tested in the dehydrogenation of isobutane at 590 °C under atmospheric pressure and were characterized by BET, XPS, TPR, XRD and RAMAN. It is found that the electron interaction exists between V and Sn oxide species on the surface of support. The doping of appropriate amount of SnO_2 leads to that the surface vanadia of catalysts is more reduced and is more highly dispersed than undoped catalyst. V_2O_5/γ-Al_2O_3 catalyst with 3 wt.% of SnO_2, exhibited higher reactivity in dehydrogenation of isobutane to isobutene.

Keywords: Vanadium oxide catalyst; SnO_2; Isobutane; Dehydrogenation; Isobutene

1. Introduction

Supported vanadium oxides have been studied for a long time as catalysts for several reactions like selective oxidation of hydrocarbons, ammoxidation, selective catalytic reduction (SCR) of NO_x with NH_3, oxidative dehydrogenation and dehydrogenation of light alkanes to the corresponding alkenes [1–18].

Depending on the specific oxide support (e.g. SiO_2, Al_2O_3, TiO_2, ZrO_2), preparation method, thermal treatment, V_2O_5 loading and presence of additives vanadia catalysts may show different catalytic activity and selectivity for oxidation and oxidative dehydrogenation of hydrocarbons [19–24]. We have already reported the dehydrogenation of isobutane to isobutene on V_2O_5/γ-Al_2O_3 by impregnation method and the effects of the addition of K and La to V_2O_5/γ-Al_2O_3 catalysts on their acidic properties and surface structures [25–28].

In the present paper, in order to enhance the activity of alumina-supported vanadia catalysts for the dehydrogenation of isobutane to isobutene, we prepared SnO_2–V_2O_5/γ-Al_2O_3 catalysts by impregnation method. The effect of SnO_2 addition on the activity of V_2O_5/γ-Al_2O_3 catalysts for the dehydrogenation of isobutane to isobutene and on the structure of catalysts was investigated by BET, XPS, TPR and RAMAN.

2. Experimental

2.1. Catalysts

The catalysts with 10 wt.% V_2O_5 loading on alumina were prepared by the impregnation method. The desired amount of $SnCl_4{\cdot}5H_2O$ and NH_4VO_3 solution was added into γ-Al_2O_3 (161 m^2/g, Beijing Research Institute of Chemical Industry), then it was dried upon stirring on water bath at 70 °C for 2 h. The samples were further dried at 120 °C for 8 h and calcined in air at 550 °C for 15 h.

2.2. Characterization

The BET surface area of the samples, S_{BET}, was obtained in an ASAP 2010 apparatus, following the BET method from N_2 (99.999%) adsorption isotherms at 77 K.

* Corresponding author. Tel.: +86 431 8499144; fax: +86 431 5262225.
E-mail addresses: fuyinghuan@sina.com (Y. Fu), m-h-c@sohu.com (H. Ma).

1381-1169/$ – see front matter © 2004 Elsevier B.V. All rights reserved.
doi:10.1016/j.molcata.2004.07.016

Temperature programmed reduction (TPR) measurements were performed in a quartz tube with 30 mg catalyst in a dried gas mixture of H_2/Ar with a ratio 1/19. The tubular furnace was linearly heated from room temperature to 900 °C at a heating rate of 15 °C/min. The hydrogen consumption was detected by thermal conductivity detector (TCD).

XPS spectra were recorded by using a VG-ESCA lab MKII spectrometer working in the constant analyzer energy mode with a pass energy of 50 eV and Mg Kα radiation as the excitation source. The C1s lines were taken as internal references.

A UV-visible Infinity Micro-Spectrometer (JY Co., France) was used to obtain Raman spectra. Raman scattering was operated at a power output of 260 mW. The samples were activated at 873 K in O_2 for 1 h and stored in a sealed glass tube prior to the measurements.

The X-ray diffraction pattern were obtained by a Shimadzu XRD-6000 diffractometer with a Nickel filtered Cu Kα radiation (λ = 0.15406 nm), power 40 KV, 30 mA.

2.3. Catalytic test

The catalytic tests were carried out in a conventional fixed bed flow apparatus. The reactor was made of a stainless steel tube, in which a thermocouple was inserted to measure the temperature of the catalyst bed. Amount of 0.5 g of catalyst was loaded in the reactor. The reaction gas was 99.9% isobutane and the space velocity was about 1000 h^{-1}. The reactant and the products were analyzed using a Shimadzu GC-8A gas chromatography with column of $AgNO_3$–benzyl at room temperature and Shimadzu C-R6A data-detector. A small amount of by-products such as methane, ethane, propane, butane, propene, 1-butene and 2-butene were detected besides isobutene.

Blank experiments were performed to find the homogeneous contributions to the net reaction. The reactor operates under isothermal, steady-state condition used in the present study. Conversion, selectivity and carbon balance are calculated by using the following formulae: (there products is also containing inconverted reactant)

$$\text{isobutane conversion (\%)} = \frac{\text{moles of isobutane converted}}{\text{moles of isobutane in feed}} \times 100$$

$$\text{isobutene selectivity (\%)} = \frac{\text{moles of isobutene formed}}{\text{moles of isobutane converted}} \times 100$$

$$\text{C-balance (\%)} = \frac{\text{moles of carbon in products}}{\text{moles of carbon in feed}} \times 100$$

Carbon balance is equal to 1 under the experimental conditions used in the present study.

3. Results and discussion

The activity of isobutane dehydrogenation over bare and SnO_2-doped V_2O_5/γ-Al_2O_3 catalysts and its specific surface area are listed in Table 1. The conversion of isobutane increases with increase of SnO_2 loading and the conversion of isobutane reaches a maximum value when the SnO_2 loading is 3 wt.%. Furthermore, the selectivity of isobutene is higher after doping SnO_2. The catalytic behavior of samples showed that the influence of SnO_2 loading in alumina-supported V_2O_5 catalysts is strong on their catalytic properties during the dehydrogenation of isobutane to isobutene. It can be found from Table 1 that specific surface area of the catalysts does not exhibit obvious change in a certain extent after doping SnO_2.

The XRD patterns of catalysts are showed in Fig. 1. The crystalline V_2O_5 was not detected in the V_2O_5/γ-Al_2O_3 and Sn-doped V_2O_5/γ-Al_2O_3 catalysts (see Fig. 1a), which suggested that vanadium oxide well dispersed on surface of support γ-Al_2O_3 when vanadium oxide loading is 10 wt.%. Whereas, the X-ray diffraction peaks of crystalline SnO_2 is found when SnO_2 loading is 7.5 wt.% for Sn-doped V_2O_5/γ-Al_2O_3(see Fig. 1a) and SnO_2 loading is 15 wt.% for SnO_2/γ-Al_2O_3(see Fig. 1b). According to the results shown in Table 1, it can be concluded that addition of excessive tin oxide results in formation of crystalline SnO_2 and decrease improving role of SnO_2 on catalytic properties of V_2O_5/γ-Al_2O_3 catalysts.

Raman spectroscopy is a very sensitive technique for the detection of both crystalline and X-ray amorphous V_2O_5, since V_2O_5 is a strong Raman scatterer. In order to better understand the effect of tin oxide on the structure of surface vanadia, Raman spectroscopy was used to characterize structure of surface vanadia.

The Raman spectra of γ-Al_2O_3, SnO_2/γ-Al_2O_3 and V_2O_5/γ-Al_2O_3 catalyst with and without SnO_2 are shown in Fig. 2. The alumina supports do not exhibit any Raman bands or only very weak ones in the 200–1200 cm^{-1} region due to the low polarizability of light atoms and the ionic character of the Al–O bonds. Raman band at 144, 199, 283, 405, 490, 524, 696 and 995 cm^{-1} is observed for V_2O_5/γ-Al_2O_3, these Raman bonds have been assigned to crystalline vanadia [16], although the presence of V_2O_5 crystallites on V_2O_5/γ-Al_2O_3 is not known from XRD studies. Spectroscopic evidence at

Table 1
Dehydrogenation of isobutane over bare and Sn-doped V_2O_5/γ-Al_2O_3 catalysts and its specific surface area

Catalysts	Conversion of isobutane (%)	Selectivity to isobutene (%)	S_{BET} (m^2/g)
Undoped	38.6	89.0	137
SnO_2 1.5 wt.%–V_2O_5/Al_2O_3	40.5	92.8	126
SnO_2 3 wt.%–V_2O_5/Al_2O_3	44.5	92.3	144
SnO_2 6 wt.%–V_2O_5/Al_2O_3	39.0	92.9	132
SnO_2 7.5 wt.%–V_2O_5/Al_2O_3	38.6	91.4	131

At 590 °C, GHSV = 1000 h^{-1}, vanadium oxide content is 10 wt.% and reacted for 30 min.

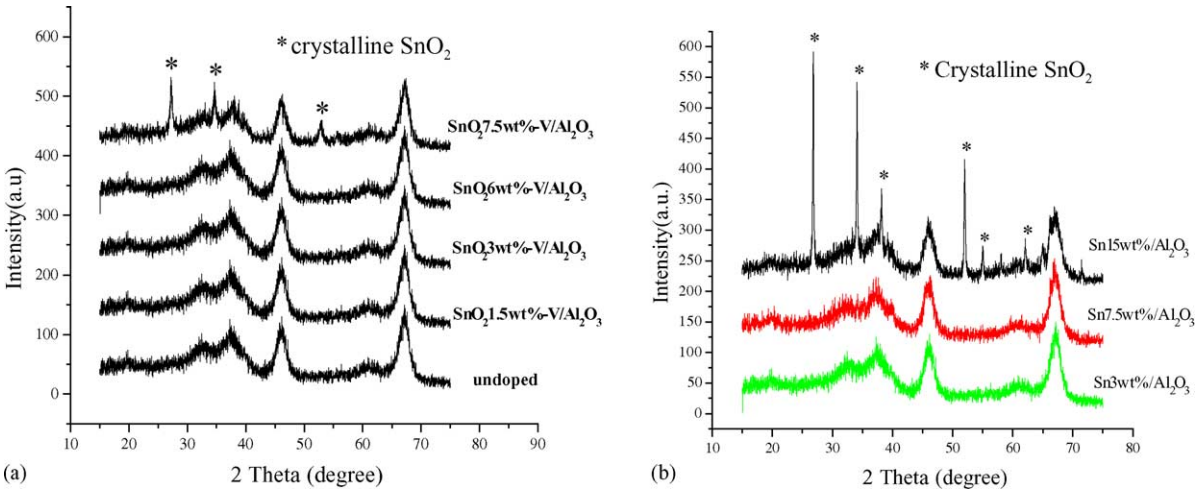

Fig. 1. XRD patterns of V_2O_5/γ-Al_2O_3, Sn-doped V_2O_5/γ-Al_2O_3 and SnO_2/γ-Al_2O_3 catalysts.

1019 cm^{-1} was also found for the presence of polymeric species [29] on the V_2O_5/γ-Al_2O_3. Whereas, the Raman bands of crystalline vanadia is not found for V_2O_5/γ-Al_2O_3 catalyst with SnO_2. Isolated monomeric vanadyl species giving rise to the obvious Raman band at 1039 cm^{-1} [30] and polymeric vanadyl species giving rise to the weak broad Raman band at (750 cm^{-1} [31,32] are observed for SnO_2 3 wt.%–V_2O_5/γ-Al_2O_3 catalyst. With SnO_2 loading rise up to 7.5 wt.%, the isolated monomeric vanadyl species giving rise to the Raman band at 1039 cm^{-1} disappears and polymeric vanadyl species giving rise to the broad Raman band at 766 cm^{-1} enhances. At one time, Raman band at 1006 cm^{-1} is attributed to polymeric vanadia species [33] is also detected for SnO_2 7.5 wt.%–V_2O_5/γ-Al_2O_3. The Raman spectra of V_2O_5/γ-Al_2O_3 catalyst with and without SnO_2 indicates that the doping of appropriate amount of SnO_2 leads to the surface vanadia of catalysts is more highly dispersed than undoped catalyst.

Furthermore, we attended also to that a obvious Raman feature of SnO_2 crystallites at (630 cm^{-1} [34,35] is observed for SnO_2 15 wt.%/γ-Al_2O_3, and that the absence of Raman feature of SnO_2 crystallites at (630 cm^{-1} for SnO_2 7.5 wt.%–V_2O_5/γ-Al_2O_3. The absence of Raman feature of SnO_2 crystallites for SnO_2 7.5 wt.%–V_2O_5/γ-Al_2O_3 is attributed to lower crystallization of SnO_2 (towards to amorphous) than in SnO_2 15 wt.%/γ-Al_2O_3 and since V_2O_5 spectrum become predominant under this conditions. This is consistent with the Herrmann et al. [34] and Ristić et al. [35] studies on Raman spectra of tin oxide.

The TPR spectra of pure SnO_2, SnO_2/Al_2O_3, V_2O_5/Al_2O_3, V_2O_5/SnO_2 and SnO_2–V_2O_5/Al_2O_3 series are shown in Fig. 3 and the corresponding TPR results are listed in Table 2. Fig. 3a shows that only one hydrogen consumption peak at 540 °C with obvious asymmestry is observed for V_2O_5 10 wt.%/γ-Al_2O_3 catalyst in the TPR profiles. Whereas, a new hydrogen consumption peak about

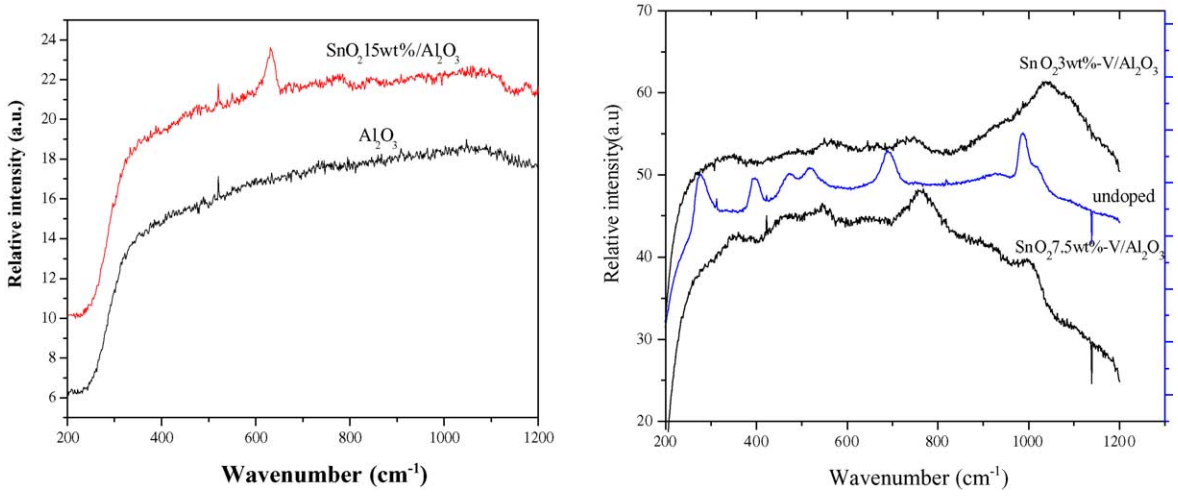

Fig. 2. Raman spectra of γ-Al_2O_3, SnO_2/γ-Al_2O_3 and V_2O_5/γ-Al_2O_3 catalyst with and without SnO_2.

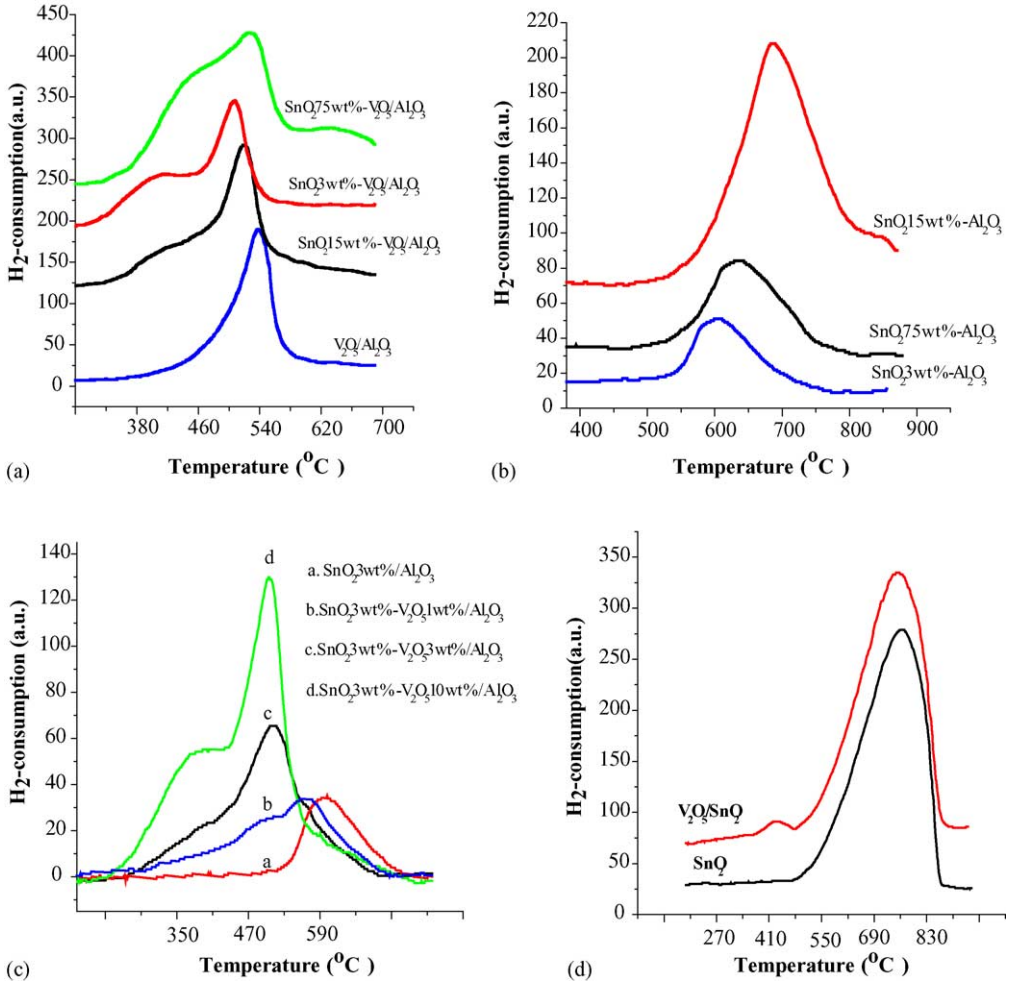

Fig. 3. TPR profile of samples.

at 400–430 °C front it is detected in the TPR profiles after addition of SnO_2. The reduction behavior of V_2O_5/γ-Al_2O_3 catalysts obviously depends on the SnO_2 loading. The reduction temperature decreased with the increase of SnO_2 loading, while the reduction temperature increases when SnO_2 loading exceed 3 wt.%. The intensity of new peak at 400–430 °C increases gradually with increase of SnO_2 loading and the third hydrogen consumption peak about at 660 °C is also found when the SnO_2 content is 7.5 wt.% (crystalline SnO_2 detected by XRD see Fig. 1a).

Regarding the attribution of three peaks, we also study in detail in present work. The TPR profiles of SnO_2/Al_2O_3 with

Table 2
Comparison of TPR Results of pure SnO_2, SnO_2/Al_2O_3, V_2O_5/Al_2O_3, V_2O_5/SnO_2 and SnO_2–V_2O_5/Al_2O_3 series

Samples	Reduction temperatures (°C)			Notes
	T_1	T_2	T_3	
SnO_2 15%/Al_2O_3			690	Crystalline SnO_2 detected by XRD
SnO_2 7.5%/Al_2O_3			630	
SnO_2 3%/Al_2O_3			600	
SnO_2 3%–V_2O_5 1%/Al_2O_3	430	500	585	
SnO_2 3%–V_2O_5 3%/Al_2O_3	430	500	580	
SnO_2 3%–V_2O_5 10%/Al_2O_3	400	500		
SnO_2 1.5%–V_2O_5 10%/Al_2O_3	430	515		
SnO_2 7.5%–V_2O_5 10%/Al_2O_3	440	530	660	Crystalline SnO_2 detected by XRD
V_2O_5 10%/Al_2O_3		540		
V_2O_5 3%/SnO_2	440		750	
SnO_2			750	

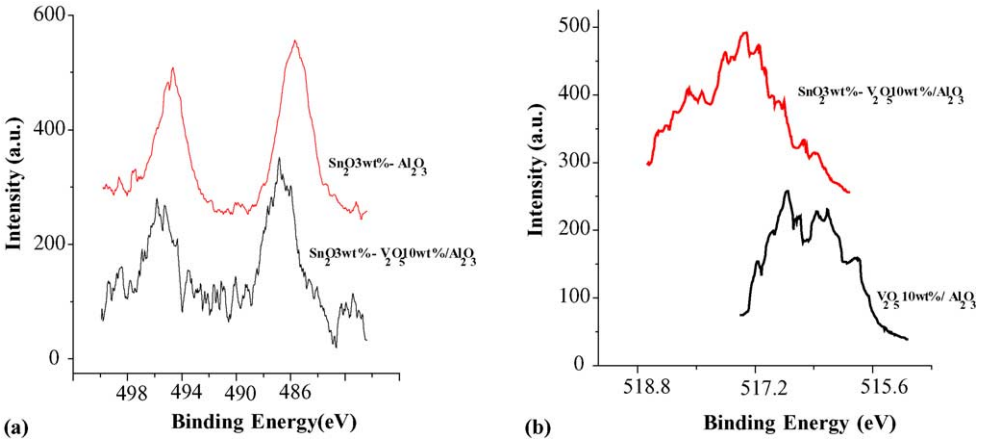

Fig. 4. XPS spectra of undoped, Sn-doped V_2O_5/γ-Al_2O_3 and SnO_2/γ-Al_2O_3.

different SnO_2 loading are shown in Fig. 2b. The reduction temperature of SnO_2 on support Al_2O_3 increases with increase of SnO_2 loading, the reduction temperature reaches 690 °C when SnO_2 loading up to 15 wt.% and that crystalline SnO_2 appears (see Fig. 1b). It is obvious that SnO_2 dispersed better on support is more reduced. By comparison of the profiles of SnO_2 7.5 wt.%–V_2O_5/γ-Al_2O_3 and SnO_2 15 wt.%/Al_2O_3, we may concluded that the third reduction peak at 660 °C is assigned to reduction of lower crystallization SnO_2 for SnO_2 7.5 wt.%–V_2O_5/γ-Al_2O_3 catalyst. Order to understanding behavior of SnO_2–V_2O_5/γ-Al_2O_3, we study also that TPR behavior of pure SnO_2, V_2O_5/SnO_2 and SnO_2 3 wt.%–V_2O_5/Al_2O_3 with different V_2O_5 loading series are shown in Fig. 3c and d. The reduction peak of amorphous SnO_2 in V_2O_5/γ-Al_2O_3 catalyst is able to shift to lower temperature with increase of V_2O_5 loading from 600 up to 580 °C and that overlap gradually with reduction of vanadia on γ-Al_2O_3 support, which results in it is hardly observed at lower SnO_2 loading (see Fig. 3c). At one time, the intensity of the reduction peaks at 400–440 and (500 °C is increases with increase of V_2O_5 loading. Moreover, Fig. 3d shows that pure SnO_2 has only one reduction peak at 750 °C and another reduction peak at 440 °C is observed except for reduction peak at 750 °C for V_2O_5/SnO_2. According to the reduction behavior of samples in Fig. 3, as well as to dates of Table 2, we hereby concluded that the first reduction peak about at 400–440 °C is assigned to reduction of vanadia on SnO_2 and the second reduction peak about at 500–540 °C is assigned to reduction of vanadia on γ-Al_2O_3 support.

The effect of Sn addition on reducibility of V_2O_5/γ-Al_2O_3 may ascribe to that the addition of SnO_2 resulted in an amorphous phase from of surface vanadia which lattice oxygen was easily released [36]. Similar TPR results once have been observed in the case of V_2O_5–SnO_2 catalysts [30,37].

Furthermore, the XPS measurements for undoped and Sn-doped V_2O_5/γ-Al_2O_3, as well as for SnO_2/γ-Al_2O_3 have been carried out and shown in Fig. 4. Fig. 4A shows that the binding energies of $Sn3d_{5/2}$ and $Sn3d_{3/2}$ due to Sn-doped V_2O_5/γ-Al_2O_3 are higher than that of SnO_2/γ-Al_2O_3. At one time, we also observed that the $V2p_{3/2}$ binding energies shift to higher values after doping Sn in Fig. 4B. The XPS experiment indicates that a strong electronic interaction occurs between Sn and V oxides at the surface of the support. This interaction leads to a higher reducibility of the Sn and V oxides with respect to the corresponding undoped ones (as shown in Fig. 3).

4. Conclusion

Thus, the electron interaction exists between V and Sn oxide species on the surface of support and appropriate amount of tin additive plays an important role in improving the dispersion and reducibility of surface vanadium oxide. Moreover, addition of SnO_2 also increases the conversion of isobutane and the isobutene selectivity on the Sn-doped V_2O_5/γ-Al_2O_3. However, higher amounts of SnO_2 lead to the formation of more unreducible agglomarated vanadia and crystalline SnO_2 and also the decreases improving role of SnO_2.

Acknowledgment

This work was supported by grant from the Natural Science Foundation of China (29873019).

References

[1] T. Blasco, J.M. López Nieto, Appl. Catal. A: Gen. 157 (1997) 117.
[2] E.A. Mamedov, C.V. Cortés, Appl. Catal. A: Gen. 127 (1995) 1.
[3] D.C.M. Dutoit, M.A. Reiche, A. Baiker, Appl. Catal. B: Environ. 13 (1997) 275.
[4] M.D. Amiridis, R.V. Duevel, I.E. Wachs, Appl. Catal. B: Environ. 20 (1999) 111.
[5] N.D. Spencer, C.J. Pereira, J. Catal. 116 (1989) 399.

[6] A. Parmaliana, F. Arena, F. Frusteri, D. Micli, V. Sokolovskii, Catal. Today 24 (1995) 231.
[7] J.L.G. Fiero, L.A. Arrua, J.M. López Nieto, G. Kremenic, Appl. Catal. 37 (1988) 323.
[8] B. Grzybowska-Swierkosz, F. Trifiro, J.C. Vedrine, Appl. Catal. A: Gen. 157 (1997) 1–420.
[9] J.L. Lakshmi, N.J. Ihasz, J.M. Miller, J. Mol. Catal. A: Chem. 165 (2001) 199.
[10] M.D. Wildberger, T. Mallat, U. Göbeo, A. Baiker, Appl. Catal. A: Gen. 168 (1998) 69.
[11] K. Hiroyuki, C.U.I. Katsumi Takahashi, J. Odenbrand, Mol. Catal. A: Chem. 139 (1999) 189.
[12] M.E. Harlin, V.M. Niemi, A.O.I. Krause, J. Catal. 195 (2000) 67.
[13] M.E. Harlin, V.M. Niemi, A.O.I. Krause, B.M. Weckhuysen, J. Catal. 203 (2001) 242.
[14] D.M. Clark, P.J.J. Tromp, P. Arnoldy, US Patent No. 5,220,092 (1993).
[15] F.M. Lee, US Patent No. 4,607,129 (1986);
F.M. Lee, US Patent No. 4,644,089 (1987).
[16] A. Khodakov, B. Olthof, A. Bell, E. Iglesia, J. Catal. 181 (1999) 205.
[17] J. López Nieto, G. Kremenic, J. Fierro, Appl. Catal. A 61 (1990) 235.
[18] J. López Nieto, J. Soler, P. Concepción, J. Herguido, M. Menéndez, J. Santamaria, J. Catal. 185 (1999) 324.
[19] A. Corma, J.M. López Nieto, N. Paredes, J. Catal. 144 (1993) 425.
[20] I.E. Wachs, B.M. Weckhuysen, Appl. Catal. A: Gen. 157 (1997) 67.
[21] G. Deo, I.E. Wachs, J. Catal. 146 (1994) 323.
[22] Q. Sun, H. Hu, R.G. Herman, et al., J. Catal. 165 (1997) 91.
[23] T. Blasco, A. Galli, J.M. Ló pez Nieto, F. Trifiró, J. Catal. 69 (1997) 203.
[24] G.C. Bond, S.F. Tahir, Appl. Catal. 71 (1991) 1.
[25] G.J. Wang, H.C. Ma, Y. Li, et al., React. Kinet. Catal. Lett. 74 (2001) 103.
[26] H.C. Ma, Z.L. Wang, W.C. Zhu, et al., Polish J. Chem. 76 (2002) 1733.
[27] H.C. Ma, Z.Y. Liu, Z.L. Wang, et al., Chem. J. Chin. U 23 (2002) 857.
[28] H.C. Ma, Y.H. Fu, Y. Li, et al., Polish J. Chem. 77 (2003) 903.
[29] X.T. Gao, S.R. Bare, J.L.G. Fierro, et al., J. Phys. Chem. B 103 (1999) 618.
[30] J.M. Jehng, J. Phys. Chem. B 102 (1998) 5816.
[31] M.A. Vuurman, I.E. Wachs, J. Phys. Chem. 96 (1992) 5008.
[32] I.E. Wachs, Catal. Today 27 (1996) 437.
[33] G.G. Cortez, M.A. Banares, J. Catal. 209 (2002) 197.
[34] J.M. Herrmann, F. Villain, L.G. Appel, Appl. Catal. A: Gen. 240 (2003) 177.
[35] M. Ristić, M. Ivanda, S. Popović, et al, J. Non-Cryst. Solids 303 (2002) 270.
[36] T. Ono, Y. Nakagawa, Y. Kubokawa, Bull. Chem. Soc. Jpn. 54 (1981) 343.
[37] X.M. Luo, Y. Chen, S.Y. Han, Chin. J. Catal. 13 (1992) 257.